


Fisher-Kolmogorov-Petrovsky-Piskunov dynamics mediated by a parent field with a delay

Steffanie Stanley and Oleg Kogan*

California Polytechnic State University, San Luis Obispo, California 93407, USA

 (Received 30 November 2020; revised 16 August 2021; accepted 18 August 2021; published 24 September 2021)

We examine a modification of the Fisher-Kolmogorov-Petrovsky-Piskunov (FKPP) process in which the diffusing substance requires a parent density field for reproduction. A biological example would be the density of diffusing spores (propagules) and the density of a stationary fungus (parent). The parent produces propagules at a certain rate, and the propagules turn into the parent substance at another rate. We model this evolution by the FKPP process with delay, which reflects a finite time typically required for a new parent to mature before it begins to produce propagules. Although the FKPP process with other types of delays have been considered in the past as a pure mathematical construct, in our paper a delay in the FKPP model arises in a natural science setting. The speed of the resulting density fronts is shown to decrease with increasing delay time and has a nontrivial dependence on the rate of conversion of propagules into the parent substance. Remarkably, the fronts in this model are always slower than Fisher waves of the classical FKPP model. The largest speed is half the classical value, and it is achieved at zero delay and when the two rates are matched.

DOI: [10.1103/PhysRevE.104.034415](https://doi.org/10.1103/PhysRevE.104.034415)

I. INTRODUCTION

Many microorganisms reproduce by means of spores. Spores are produced by a parent organism [1] and have a probability to produce a new parent organism. Consider, for example, *Puccinia graminis*—the pathogen that causes wheat stem rust plant disease [2]. After a urediniospore of *P. graminis* has successfully infected a host plant, a fungus (i.e., a parent organism) will establish and mature inside the plant for 10–15 days after which it will form postules on the surface, and they will release new spores [3]. The process repeats when the spores disperse and find another host to infect, leading to formation of new fungi (parent organisms) there, and so on. A time between the colonization of a host and production of spores by the new fungus is called latent period [4]. This type of life cycle that involves spores and a parent organism with a latent period is shared by many fungal plant pathogens [3,4] (see, for instance, Chap. 11), and it is a feature of fungi, in general [5].

More broadly, reproduction by means of spores is common in biology—for example, among algae and plants [1]. Slime molds also employ spores in their life cycle [6]. The spores are an example of what is called “propagules” in ecology [7].

The population dynamics of reproducing microorganisms often gives rise to propagating density fronts [8,9]. The dynamics of fronts of organisms that reproduce by direct division can be described by the Fisher-Kolmogorov-Petrovskiy-Piscunov (FKPP) model. This well-known model originated in the context of population genetics [10,11] but has found applications in fields as diverse as biochemical waves during development to nuclear physics [9,12–16].

The FKPP model is a simple reaction-diffusion equation that reads

$$\dot{\phi} = f(\phi) + D\phi'', \quad (1)$$

where $f(\phi)$ is a growth model—for instance, logistic growth $f(\phi) = \delta\phi(1 - \phi)$. In the context of population dynamics, the density field ϕ represents the density (per unit length) of diffusing microorganisms—such as bacteria—which also reproduce themselves with rate δ . An isolated region of space inoculated at initial moment leads to the development of propagating density fronts, known as Fisher waves.

Recently, the role of delay in FKPP model has been examined [17–21]. However, in these papers the delay has been introduced by modifying the growth function to have the form $\delta\phi(t)[1 - \phi(t - \tau)]$. Although the study of the dynamics of fronts that result from this is an interesting mathematical exercise, this is not necessarily the most natural way in which delay would arise physically.

On the other hand, delay occurs naturally in scenarios that involves propagules and parent organisms. In these situations, the particles do not reproduce themselves, and it would be unrealistic to apply the FKPP model with a single density field to such biological settings. Instead, propagules produce parent organisms, which, after a latent period produce new propagules, so this requires two separate density fields—for propagules and parents, respectively. Thus, a more appropriate basic model for this scenario would be as follows [22]:

$$\dot{\phi} = \delta\theta(t - \tau) + D\phi'' - \gamma\phi, \quad (2)$$

$$\dot{\theta} = \gamma\phi \left(1 - \frac{\theta}{\theta_{\max}}\right), \quad (3)$$

where we explicitly remind the reader that the function θ in Eq. (2) is evaluated at time $t - \tau$; all the other terms are evaluated at time t . Here ϕ is the usual density of the propag-

*okogan@calpoly.edu

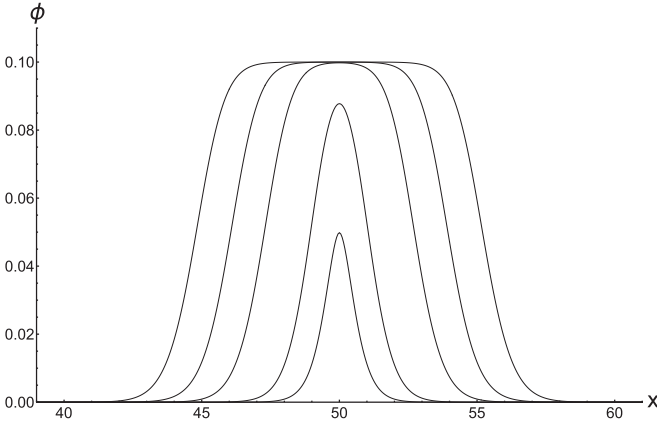


FIG. 1. (a) Density wave ϕ vs x at $t = 1.98, t = 5.94, t = 11.88, t = 15.84,$ and $t = 19.8$. The parameters are $\Gamma = 10, \mathcal{T} = 1$. The δ -function initial condition at $t = 0$ is not shown.

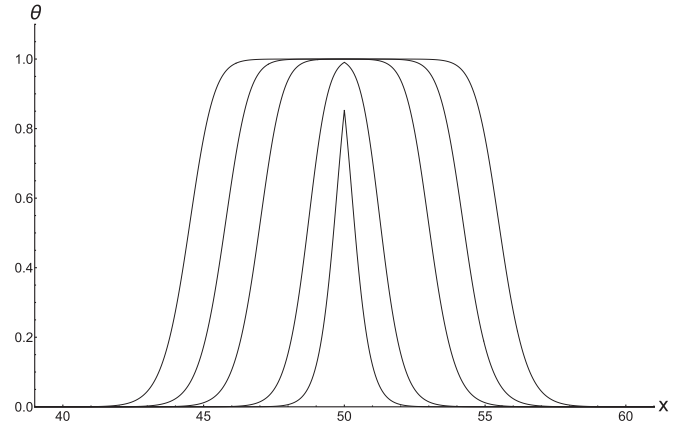


FIG. 2. Density wave θ vs x at $t = 1.98, t = 5.94, t = 11.88, t = 15.84,$ and $t = 19.8$. The parameters are $\Gamma = 10, \mathcal{T} = 1$.

ules, whereas θ represents the density of a parent organism, such as fungi. The parent is immobile—it grows on some substrate, such as soil. However, the propagules can diffuse—again, reflecting the typical biological scenario in which this dynamics arises. The rate γ is the probability per unit time that a propagule turns into a parent—for example, a spore giving rise to a new fungus, and δ is the rate at which the parent substance produces propagules—for example, the rate at which fungi spew out spores. Thus, the mobile propagules produce the immobile parent (with rate γ), which, in turn, produces new propagules.

However, propagule production usually happens with a delay, because the parent needs to reach a certain stage of maturity before producing propagules. The quantity τ is the delay time, commonly referred to in biological literature as the “latent time.” A time τ must pass between the moment when a propagule has turned into a new parent substance and the moment when this parent begins to produce new spores. In the mean time, new propagules are deposited. Therefore, the rate of fungal production at time t is not $\delta\theta(x, t)$, but $\delta\theta(x, t - \tau)$. Thus, the notation $\theta(t - \tau)$ in Eq. (2) is a reminder that θ in that term is evaluated at time $t - \tau$, whereas all the other terms are evaluated at t (the coordinate argument x is suppressed). Finally, the parent substance typically has a carrying capacity—a maximal density θ_{\max} at which it will stop growing.

In our paper we will investigate the behavior of density waves in this model, focusing, in particular, on the dependence of the speed of density fronts upon the model parameters.

First, we rescale variables to lower the number of relevant parameters. Note that δ sets a natural timescale for this problem, namely, $1/\delta$. Therefore, we define dimensionless time by $\tilde{t} = \delta t$. This is equivalent to measuring time not in seconds, but in units of $1/\delta$. Also, the diffusion coefficient has dimensions of $\frac{\text{distance}^2}{\text{time}}$. Therefore, a natural distance scale is $\sqrt{\frac{D}{\delta}}$, and we define a dimensionless coordinate $\tilde{x} = x\sqrt{\frac{\delta}{D}}$. Finally, we define dimensionless densities by $\tilde{\phi} = \frac{\phi}{\theta_{\max}}$ and $\tilde{\theta} = \frac{\theta}{\theta_{\max}}$. This is equivalent to expressing densities as a fraction of the maximal parent density. Substituting all these variables we

have

$$\dot{\tilde{\phi}} = \tilde{\theta}(\tilde{t} - \mathcal{T}) + \tilde{\phi}'' - \Gamma\tilde{\phi}, \quad (4)$$

$$\dot{\tilde{\theta}} = \Gamma\tilde{\phi}(1 - \tilde{\theta}). \quad (5)$$

The derivatives are with respect to new dimensionless variables. We are left with only two parameters. The first is the dimensionless infection rate Γ , which is given by $\Gamma = \gamma/\delta$ in terms of the physical parameters. The second is the dimensionless latent time \mathcal{T} , which is given by $\mathcal{T} = \tau\delta$ in terms of the physical parameters.

The resulting speeds of fronts would also be dimensionless, \tilde{v} . It will be a function of Γ and \mathcal{T} . To switch back to the original physical variables, the dimensionless speed must be multiplied by $\frac{\sqrt{D/\delta}}{1/\delta} = \sqrt{\delta D}$. In other words, the speed in physical units is given by

$$v = \tilde{v}(\gamma/\delta, \tau\delta)\sqrt{\delta D}. \quad (6)$$

In the classical case, \tilde{v} has a value of 2. In the present model \tilde{v} is a function of γ/δ and $\tau\delta$ and represents the departure from the classical FKPP result. We examine this difference.

II. RESULTS

A. Front examples

We will drop \sim to lighten the notation but will switch back where necessary when presenting results. Figures 1 and 2 show examples of propagating density waves that result out of the initial condition $\phi(x, t = 0) = \delta(x - x_0)$ and $\theta(x, t = 0) = 0$. We see that after an initial transient, a pair of uniformly moving fronts are launched. In the rest of the paper we will be concerned only with these uniformly moving fronts.

B. Front speeds

We now derive theoretical predictions for front speeds and compare them with numerical results. This is a standard analysis that follows [23].

First, we assume that a uniformly traveling front (UTF) exists for which $\theta(x, t) = \theta(x - vt)$ and $\phi(x, t) = \phi(x - vt)$. Thus, we seek a UTF solution by substituting this ansatz into

equations of motion (4) and (5). We get

$$-v \frac{d\phi}{dz} = \theta(z + v\mathcal{T}) + \frac{d^2\phi}{dz^2} - \Gamma\phi, \quad (7)$$

$$-v \frac{d\theta}{dz} = \Gamma\phi(1 - \theta), \quad (8)$$

where $z = x - vt$. The UTF is described by a system of ordinary differential equations. The equations have a fixed point at $(\theta = 0, \phi = 0)$ —corresponding to the leading edge of the front and a fixed point at $(\theta = 1, \phi = 1/\Gamma)$ —corresponding to the trailing edge of the front. The solution near the $(0,0)$ fixed point determines the shape of the leading edge.

Next, we assume that fronts are pulled [23], which means that their speed is determined by the leading edge where the nonlinear terms are negligible. The pulled assumption will be validated through comparison with numerical predictions of Eqs. (4) and (5). Thus, the leading edge is described by the linearized equations,

$$-v \frac{d\phi}{dz} = \theta(z + v\mathcal{T}) + \frac{d^2\phi}{dz^2} - \Gamma\phi, \quad (9)$$

$$-v \frac{d\theta}{dz} = \Gamma\phi. \quad (10)$$

The solution will have the form $\phi = \phi_0 e^{-\lambda z}$ and $\theta = \theta_0 e^{-\lambda z}$. Substituting this into the linearized equations produces a relationship,

$$\frac{\Gamma e^{-v\lambda\mathcal{T}}}{v\lambda} - (v\lambda) - (\Gamma - \lambda^2) = 0, \quad (11)$$

which relates the front speed v and the decay length of the front λ , i.e., it gives a function $v(\lambda)$. The theory of [23] states that for initial conditions (ICs) that decay in space faster than an exponential with a certain critical decay rate, the UTF solution will have a λ that minimizes $v(\lambda)$. All localized ICs, such as a δ -function IC satisfy this criterion. This minimum will take place at λ^* , and the front speed will be $v^* = v(\lambda^*)$.

Taking the derivative of Eq. (11) and solving for $v'(\lambda)$ gives

$$v'(\lambda) = -v(\lambda) \frac{\Gamma + \lambda v(\lambda) \{ \Gamma \mathcal{T} - \lambda e^{\lambda \mathcal{T} v(\lambda)} [2\lambda - v(\lambda)] \}}{\lambda [\Gamma + \Gamma \mathcal{T} \lambda v(\lambda) + \lambda^2 v^2(\lambda) e^{\lambda \mathcal{T} v(\lambda)}]}. \quad (12)$$

This is zero when the numerator is zero. Thus, we can, in principle, solve for $v(\lambda)$ from Eq. (11), substitute into the numerator, set it to zero, and find λ^* . Alternatively, we can treat v^* and λ^* as two independent variables and find them from a simultaneous solution of Eq. (11) and the numerator = 0, i.e.,

$$\Gamma e^{-v^* \lambda^* \mathcal{T}} - (v^* \lambda^*)^2 - v^* \lambda^* [\Gamma - (\lambda^*)^2] = 0, \quad (13)$$

$$\Gamma + \lambda^* v^* [\Gamma \mathcal{T} - \lambda^* e^{\lambda^* \mathcal{T} v^*} (2\lambda^* - v^*)] = 0. \quad (14)$$

This was performed numerically for a set of Γ and \mathcal{T} . Reverting back to the dimensionless notation, this produces $\tilde{v}(\Gamma, \mathcal{T})$. The result is plotted in Fig. 3 for several Γ s and \mathcal{T} s. Figure 4 compares these theoretical predictions with front speeds obtained from the numerical solution of Eqs. (4) and (5). The details of our numerical approach can be found in Appendix A.

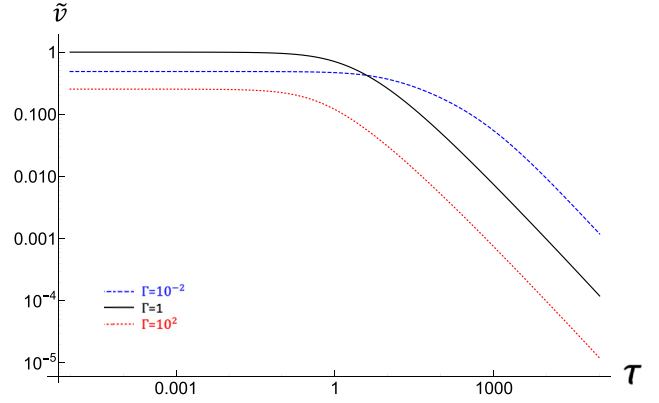


FIG. 3. Dimensionless speed \tilde{v} vs dimensionless latent times \mathcal{T} for various dimensionless infection rates Γ .

C. Analysis

Figure 3 demonstrates that our results have three main features. The first, is the limiting speed as \mathcal{T} goes to zero. The second, is the large \mathcal{T} asymptotic regime, where $\tilde{v}(\mathcal{T})$ appears to have an asymptotic behavior reminiscent of a power law (we show below that it is not a pure power law). The third, is the characteristic crossover point beyond which this asymptotic approximation is valid. This crossover point is a function of Γ . We now extract these properties.

1. Zero delay

First, we study the speed at zero delay. Setting $\mathcal{T} = 0$ in Eqs. (13) and (14) we can produce an analytic result. There are four roots, but only one of which is positive and real. In dimensionless notation, this root is given by

$$\tilde{v}(\Gamma) = \frac{[6 + \Gamma - \sqrt{\Gamma(3 + \Gamma)}] \sqrt{-3\Gamma + 6\sqrt{\Gamma(3 + \Gamma)}}}{3(4 + \Gamma)}. \quad (15)$$

This function is plotted in Fig. 5. At small Γ this function behaves as $\frac{3^{3/4}}{\sqrt{2}} \Gamma^{1/4}$. At large Γ , it approaches the asymptotic behavior $\frac{3^{3/2}}{2} \Gamma^{-1/2}$. The speed reaches the maximum value of 1 at $\Gamma = 1$.

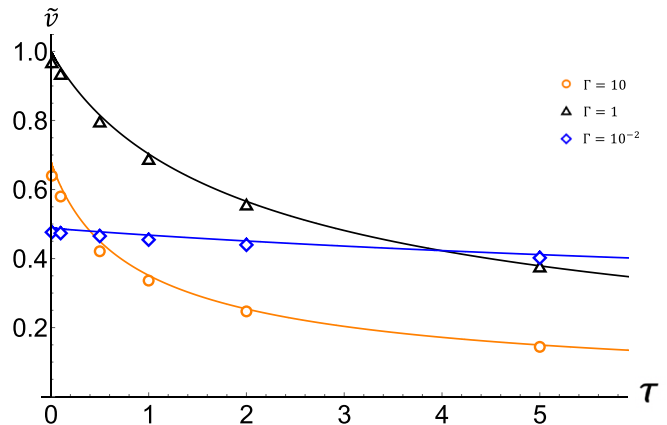


FIG. 4. Comparison of theoretical $\tilde{v}(\mathcal{T})$ with values extracted from the numerical solution of Eqs. (4) and (5) for three different values of Γ .

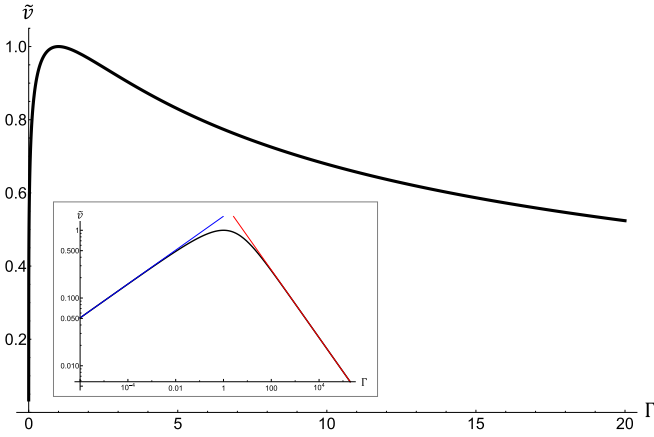


FIG. 5. Dimensionless speed $\tilde{v}(\Gamma)$ at zero delay \mathcal{T} . The inset: The same quantity on a log-log scale. The two thin lines are the low- and high- Γ asymptotics, $\frac{3^{3/4}}{\sqrt{2}}\Gamma^{1/4}$ (blue) and $\frac{3^{3/2}}{2}\Gamma^{-1/2}$ (red) respectively.

At $\Gamma = 0$, the parent density is static, and the propagule density obeys a driven diffusion equation – not FKPP model – and does not admit UTF solutions; this is the meaning of zero front speed. On the other hand, as Γ approaches infinity we also do not recover the FKPP model, because whereas the rate of conversion from propagules to the substrate density goes to infinity, the rate of production of new propagules remains 1. Therefore, this is effectively equivalent to killing of propagules with infinite rate, giving a speed zero. So, we see that the model does not match with the KFPP model in either limit. The optimal speed is achieved at intermediate $\Gamma = 1$, but there is no reason for it to reach the KFPP value of $\tilde{v} = 2$ since in this intermediate regime the model is clearly not equivalent to the FKPP model.

Evidently, this model does not reproduce the FKPP results for any parameters, and there is no reason to expect a correspondence because the propagule production terms are different. For instance, the localized dynamics in the absence of transport is a first order in time in the classical FKPP case, but it is second order in time in the new model.

2. Finite delay

Turning on a finite delay slows down the front as we can see from Fig. 3. To understand the large- \mathcal{T} asymptotic behavior, we noticed from numerical calculations of solutions to Eqs. (13) and (14) that the product $v^*\lambda^*\mathcal{T}$ tends to a number greater than 1 as $\mathcal{T} \rightarrow \infty$ for any Γ . Also, v^* goes to zero, whereas λ^* does not. With the help of this observation, Eqs. (13) and (14) at large \mathcal{T} read

$$(v^*\lambda^*) - \Gamma + (\lambda^*)^2 = 0, \tag{16}$$

$$\Gamma - 2v^*(\lambda^*)^3 e^{\lambda^*\mathcal{T}v^*} = 0. \tag{17}$$

The first equation gives $\lambda^* = \frac{1}{2}[v^* \pm \sqrt{(v^*)^2 + 4\Gamma}]$, and we must choose the positive root because only this choice always produces a positive λ^* . It is convenient to factor out the quantity $2\sqrt{\Gamma}$ from the speed, so we let $v^* = 2\sqrt{\Gamma}w$. Substituting both of these expressions into the second equation

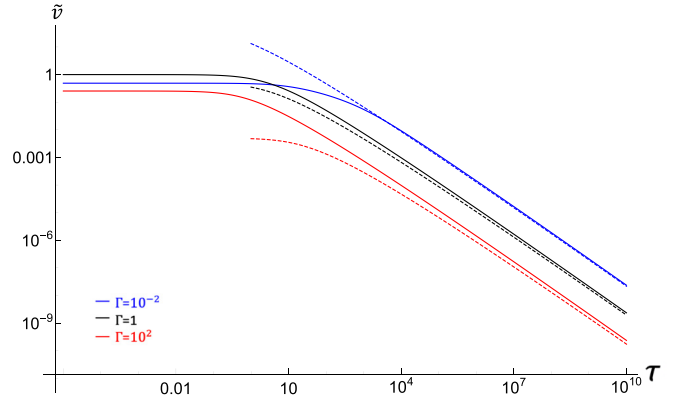


FIG. 6. Tails of $\tilde{v}(\mathcal{T})$ given by Eq. (20)—dashed curves, compared with the exact result, obtained from Eqs. (13) and (14)—solid curves.

gives

$$4\Gamma^{3/2}w(w + \sqrt{w^2 + 1})e^{(2\Gamma\mathcal{T})w(w + \sqrt{w^2 + 1})} = 1. \tag{18}$$

Now, an equation of the form $1 = aue^{bu}$ has a solution $u = \frac{W(b/a)}{b}$, where W is a Lambert W function, or product logarithm. Therefore, we have

$$w(w + \sqrt{w^2 + 1}) = \frac{W(\frac{\mathcal{T}}{2\sqrt{\Gamma}})}{2\Gamma\mathcal{T}}. \tag{19}$$

This has a solution,

$$w = \frac{W(\frac{\mathcal{T}}{2\sqrt{\Gamma}})}{2\Gamma\mathcal{T}\sqrt{1 + \frac{w(\frac{\mathcal{T}}{2\sqrt{\Gamma}})}{\Gamma\mathcal{T}}}} \approx \frac{W(\frac{\mathcal{T}}{2\sqrt{\Gamma}})}{2\Gamma\mathcal{T}}.$$

So, the high- Γ tail of the dimensionless speed is given by

$$\tilde{v} = \frac{W(\frac{\mathcal{T}}{2\sqrt{\Gamma}})}{\sqrt{\Gamma}\mathcal{T}}. \tag{20}$$

We compare predictions of this equation with exact results in Fig. 6. Evidently, the tail behavior of $\tilde{v}(\mathcal{T})$ is not a pure power law. We can estimate the crossover point approximately by equating the value at zero τ given by Eq. (15) and the denominator of Eq. (20). The result is a complicated function

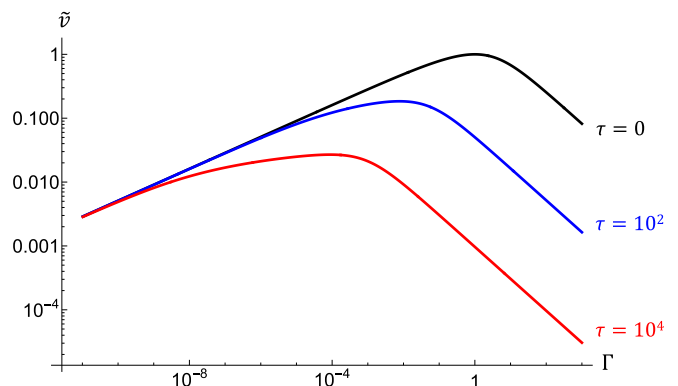


FIG. 7. Dimensionless speed $\tilde{v}(\Gamma)$ at various delay \mathcal{T} on a log-log scale. The $\mathcal{T} = 0$ curve is the same as in Fig. 5.

that diverges at small Γ as $\frac{\sqrt{2}}{3^{3/4}}\Gamma^{-3/4}$ and tends to a value of ≈ 0.3849 as $\Gamma \rightarrow \infty$.

Finally, we also provide in Fig. 7 a function $\tilde{v}(\Gamma)$, similar to Fig. 5. The black curve is the same as the inset in our Fig. 5, and the other two curves plot this function for larger \mathcal{T} . Thus, when the value of the delay is held fixed—however large—the speed does go to zero as $\Gamma \rightarrow 0$.

III. CONCLUSION

The largest speed in our model is $\sqrt{\delta D}$, which is achieved at zero delay and when the rate of conversion from propagules to parent is matched to the rate at which the parent produces propagules. This speed is exactly 1/2 of the classical Fisher speed, although one must be careful to take this comparison at face value since the terms that model production of new material are different in the two models. Although propagules are produced by a parent organism in the new model, they are produced by other propagules in the basic FKPP model. Still, the factor $\sqrt{\delta D}$ in the expression for front speed naturally arises in both models on dimensional grounds, although it is multiplied by different factors in the two models.

Thus, we find that propagating fronts in organisms that require a parent for reproduction will move at most half as slowly as fronts in organisms that reproduce themselves. All other common rates being equal, bacterial fronts will move twice as fast as fungal fronts.

When the rate of propagule production by the parent does not equal to the rate of conversion from propagules to the parent, the front speed is slower than this optimal value. Increasing conversion rate past the production rate decreases front speed. For sufficiently large conversion rate, the speed of the front—or, equivalently, the rate at which the amount of biomass grows—scales as conversion rate to the power $-1/2$. This is reminiscent of an effect that was recently described in a completely different field. The authors of Ref. [24] describe an open quantum system of free fermions driven by a source that injects fermions. When the injection rate is sufficiently large, the rate at which the number of fermions in the system grows scales inversely with the injection rate. The authors explain that this is a manifestation of the quantum Zeno effect. Moreover, our Fig. 5 over the entire range of Γ resembles Fig. 1 in Ref. [24] over the entire range of injection rates.

As one would expect, the delay further slows down the propagation of fronts. We find that for sufficiently large delay, the front speed scales approximately inversely with the delay time, although a more exact result introduces nonpower law corrections.

ACKNOWLEDGMENTS

We would like to thank William and Linda Frost Fund for supporting undergraduate research at Cal Poly.

APPENDIX A: NUMERICAL METHOD

Our numerical method uses a first-order time-differencing scheme, for example,

$$\left. \frac{\partial \phi}{\partial t} \right|_{x,t_n} \rightarrow \frac{\phi(x_m, t_{n+1}) - \phi(x_m, t_n)}{\Delta t} \quad (\text{A1})$$

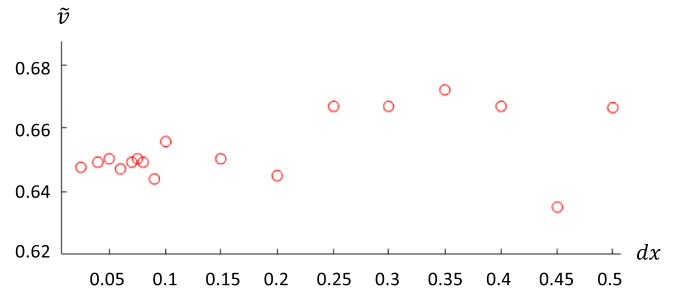


FIG. 8. Front speed as a function of dx for $\mathcal{T} = 1$, $\Gamma = 1$, and simulation time $T = 15$.

and an upwind spatial differencing scheme,

$$\left. \frac{\partial \phi}{\partial x} \right|_{x_m, t_n} \rightarrow \frac{\phi(x_m, t_n) - \phi(x_{m-1}, t_n)}{\Delta x} \quad (\text{A2})$$

applied to Eqs. (4) and (5) (we continue to suppress \sim for readability). Here $x_m = x_0 + m \Delta x$ and $t_n = t_0 + n \Delta t$. The integration was performed over a finite spatial interval with an initial condition placed in the center. At the extreme left and extreme right points of this spatial interval, we set the values of both densities to zero. However, the spatial domain was chosen large enough so that neither front ever came close to either boundary given the placement of the initial profile.

We performed convergence test for select parameter combinations. An example is shown in Fig. 8. The front speed generated by the simulation code does not show a strong dependence on Δx . All the results presented in the paper were obtained with $\Delta x = 0.05$, which is much less than the typical characteristic width of fronts. To ensure stability, we chose $\Delta t = 0.25(\Delta x)^2$ as suggested by an earlier paper on a similar model [25]. Instabilities were not observed. To extract the speed of the wavefronts from these simulations, we tracked the position of the contour of a fixed reference density, chosen to lie in the leading edge. There is a transient time period during which the shapes of fronts develop. During this same transient period the speed of fronts also changes. As time progresses, the front profiles tend to a stationary shape, and front speeds tend to a limiting value. This limiting value will be identical for both densities ϕ and θ , although instantaneous front speeds of the two densities are generally not identical during the transient period.

The rate of convergence to the limiting speed depends on parameters. We needed to develop a consistent method of scaling the total run time T with this convergence rate and to ensure the simulations ran long enough for density profiles to come close enough to the asymptotic speed. In order to make this choice, we used the following idea. Starting from a δ -function IC, the ϕ profile very quickly diffuses and the maximal value rapidly decreases. At a certain instant of time t^* it reaches the smallest value after which the ϕ profile grows again. This is a characteristic time at which the growth mechanism becomes important. We display t^* vs \mathcal{T} in Fig. 9. We used t^* as a characteristic measure of the transient time. Figure 10 demonstrates the measured speed of the front as a function of the total simulation time T , expressed as multiples of t^* for a particular Γ and \mathcal{T} . Here, we see that the front speed maintains an upward trend for greater T and saturates to

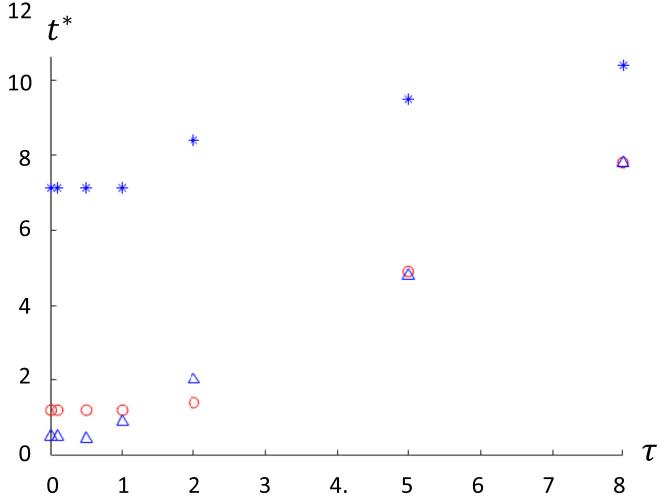


FIG. 9. t^* as a function of \mathcal{T} . Blue asterisks: $\Gamma = 10^{-2}$, red circles: $\Gamma = 1$, blue triangles: $\Gamma = 10$.

an equilibrium value for sufficiently large T . The simulation time T was chosen to be a factor of 40 larger than t^* [a linear fit to $t^*(\mathcal{T})$ was used over a range of \mathcal{T} s]. The number 40 was chosen as a compromise between a sufficiently small error from the theory and a practical simulation time since increasing T increases the simulation time dramatically. We repeated the procedure for $\Gamma = 10^{-2}$ and $\Gamma = 10$, although the scaling factor of 20 was used for $\Gamma = 10^{-2}$ —it gave a sufficient accuracy in comparison with the theoretical curve.

APPENDIX B: SATURATION DYNAMICS

Here we demonstrate that profile densities behind fronts saturate to their maximum values without oscillations. In seeking the UTF, we substituted the ansatz $\theta(x, t) = \theta(x - vt)$ and $\phi(x, t) = \phi(x - vt)$ into Eqs. (4) and (5) of our paper. This resulted in Eqs. (7) and (8). We would like to emphasize that the full solution of Eqs. (4) and (5) does not have this form since it has two fronts spreading in opposite directions. The UTF describes the shape and speed of each front if it attains

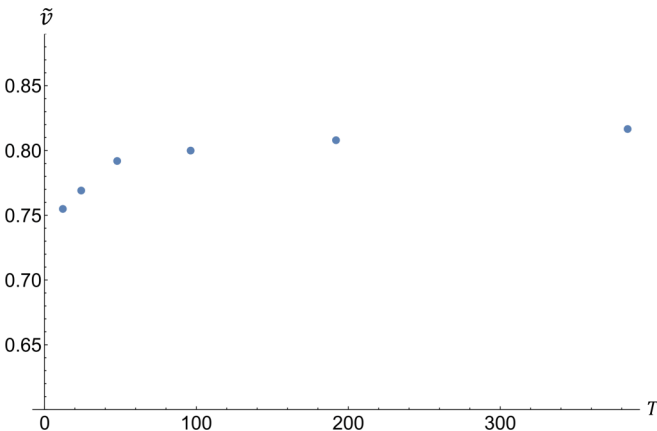


FIG. 10. Front speed \tilde{v} vs the total simulation time T for $\Gamma = 1$ and $\tau = 0.5$. The data points are calculated for $T = 10t^*$, $T = 20t^*$, $T = 40t^*$, $T = 80t^*$, $T = 160t^*$, $T = 320t^*$.

a constant speed and shape (the validity of the UTF ansatz is checked by comparing predictions of front speeds with simulations, such as in Fig. 4). In other words, the solution to Eqs. (7) and (8) represent what a comoving observer running along with the front would see at times when the distance between fronts becomes much larger than their width.

The dynamical system represented by Eqs. (7) and (8) has two fixed points that satisfy

$$\begin{aligned} 0 &= \theta^* - \Gamma\phi^*, \\ 0 &= \Gamma\phi^*(1 - \theta^*). \end{aligned}$$

These fixed points are as follows: $(\theta^* = 0, \phi^* = 0)$ and $(\theta^* = 1, \phi^* = \frac{1}{\Gamma})$. The first represents the leading edge of the front (i.e., the part of the front ahead of the direction of its motion), and the second represents the saturated value.

The shape of the front is given by the heteroclinic solution of Eqs. (7) and (8) that connects the $(\theta^* = 1, \phi^* = \frac{1}{\Gamma})$ fixed point with the $(\theta^* = 0, \phi^* = 0)$ fixed point [23]. In describing the right-moving front, where $z \rightarrow \infty$ corresponds to going ahead to the leading edge, such a heteroclinic trajectory leaves the $(1, \frac{1}{\Gamma})$ fixed point at $z = -\infty$ and arrives at the $(0, 0)$ fixed point at $z = +\infty$.

We expand Eqs. (7) and (8) around the $(1, \frac{1}{\Gamma})$ fixed point. Let $\theta = 1 + X$ and $\phi = \frac{1}{\Gamma} + Y$. The result is

$$-vY' = X(z + v\mathcal{T}) + Y'' - \Gamma Y, \quad (\text{B1})$$

$$-vX' = -X - \Gamma XY. \quad (\text{B2})$$

Here the prime represents differentiation with respect to z , and the first term on the right hand side of the first equation means evaluate X at $z + v\mathcal{T}$. We are interested in the dynamics around $X = Y = 0$, so we keep only the linear terms. Also, let $Y' = U$. Therefore, we are concerned with the dynamics of the linear delayed system given by

$$Y' = U, \quad (\text{B3})$$

$$U' = -vU + \Gamma Y - X(z + v\mathcal{T}), \quad (\text{B4})$$

$$X' = \frac{X}{v}. \quad (\text{B5})$$

We now seek the exponential ansatz that represents the departure from the saturated state. Let

$$\begin{pmatrix} U \\ X \\ Y \end{pmatrix} = \begin{pmatrix} a \\ b \\ c \end{pmatrix} e^{\mu z}.$$

Substituting this into the system (B3)–(B5) and rearranging terms we get

$$\begin{pmatrix} 1 & 0 & -\mu \\ \mu + v & e^{\mu v \mathcal{T}} & -\Gamma \\ 0 & \mu - \frac{1}{v} & 0 \end{pmatrix} \begin{pmatrix} a \\ b \\ c \end{pmatrix} = \begin{pmatrix} 0 \\ 0 \\ 0 \end{pmatrix}. \quad (\text{B6})$$

The eigenvalues are $\mu_1 = \frac{1}{v}$ and $\mu_{\pm} = \frac{-v \pm \sqrt{v^2 + 4\Gamma}}{2}$. Two of the eigenvalues are positive, and one is negative. The eigenvectors (not calculated here) corresponding to the positive eigenvalues span the space of the unstable manifold of the fixed point $(\theta^* = 1, \phi^* = \frac{1}{\Gamma})$. The heteroclinic trajectory leading into the $(\theta^* = 0, \phi^* = 0)$ fixed point should lie on this

unstable manifold [26]. Because the eigenvalues are real, there are no oscillations around the saturated state. Thus, there is

never “overshooting” around the maximal density left behind moving fronts.

-
- [1] M. Petruzzello, *Encyclopaedia Britannica Online*, s.v. Spore (Encyclopedia Britannica, Chicago, 2019), <https://www.britannica.com/science/spore-biology> (accessed October 29, 2020).
- [2] Data from Cereal Disease Laboratory. Retrieved on August 15, 2021 from <https://www.ars.usda.gov/midwest-area/stpaul/cereal-disease-lab/docs/cereal-rusts/wheat-stem-rust/>.
- [3] G. N. Agrios, *Plant Pathology*, 5th ed. (Elsevier Academic, Amsterdam/Boston, 2005).
- [4] *The Cereal Rusts, Volume II: Diseases, Distribution, Epidemiology, and Control*, edited by A. P. Roelfs and W. R. Bushnell (Academic, Orlando, 1985).
- [5] J. Deacon, *Fungal Biology*, 4th ed. (Blackwell, Malden, MA, 2006).
- [6] J. T. Bonner, *The Social Amoebae: The Biology of Cellular Slime Molds* (Princeton University Press, Princeton, 2009).
- [7] Propagule. (2019). Retrieved October 29, 2020 from <https://en.wikipedia.org/wiki/Propagule>.
- [8] D. R. Nelson, *Annu. Rev. Biophys.* **41**, 371 (2012).
- [9] J. Murray, *Mathematical Biology. I: An Introduction* (Springer, California, 2003).
- [10] R. A. Fisher, *Ann. Eugenics* **7**, 355 (1937).
- [11] A. Kolmogorov, I. Petrovsky, and N. Piskunov, *Moscow Univ. Bull. Math.* **1**, 1 (1937).
- [12] J. F. Douglas, K. Efimenko, D. A. Fischer, F. R. Phelan, and J. Genzer, *Proc. Natl. Acad. Sci. USA* **104**, 10324 (2007); A. R. Kerstein, *J. Stat. Phys.* **45**, 921 (1986).
- [13] S. N. Majumdar and P. L. Krapivsky, *Physica A* **318**, 161 (2003).
- [14] B. Derrida and H. Spohn, *J. Stat. Phys.* **51**, 817 (1988)
- [15] D. Carpentier and P. Le Doussal, *Nucl. Phys. B* **588**, 565 (2000).
- [16] C. Marquet, R. Peschanski, and G. Soye, *Phys. Rev. D* **73**, 114005 (2006); S. Munier and R. Peschanski, *Phys. Rev. Lett.* **91**, 232001 (2003); I. Balitsky, *Nucl. Phys. B* **463**, 99 (1996); Y. V. Kovchegov, *Phys. Rev. D* **60**, 034008 (1999); **61**, 074018 (2000); C. Marquet, R. Peschanski, and G. Soye, *Nucl. Phys. A* **756**, 399 (2005).
- [17] A. Gomez, S. Trofimchuk, *J. Differ. Equations* **250**, 1767 (2011).
- [18] X. Zou, *J. Comput. Appl. Math.* **146**, 309 (2002).
- [19] S. V. Aleshin, S. D. Glyzin, and S. A. Kaschenko, *Model. Anal. Inf. Syst.* **22**, 304 (2015).
- [20] S. V. Aleshin, S. D. Glyzin, and S. A. Kaschenko, *Doklady Math.* **96**, 636 (2017).
- [21] S. V. Aleshin, S. D. Glyzin, and S. A. Kaschenko, *J. Phys.: Conf. Ser.* **681**, 012023 (2016).
- [22] This model is most appropriate for asexual propagules, such as spores.
- [23] W. van Saarloos, *Phys. Rep.* **386**, 29 (2003)
- [24] P. L. Krapivsky, K. Mallick, and D. Sels, *J. Stat. Mech.* (2019) 113108.
- [25] O. Kogan, K. O’Keeffe, and C. R. Myers, *Phys. Rev. E* **96**, 022220 (2017).
- [26] The fact that the $(1, \frac{1}{v})$ fixed point is unstable in the dynamical system (B3)–(B5) should not be confused with the fact that it is a stable (saturating) state in the original partial differential equations that describe the density profiles. The dynamical system (B3)–(B5) with a time variable z only produces the shape of the front.